Precision Rydberg state spectroscopy with slow electrons and the proton-radius puzzle

Ulrich D. Jentschura [1] and Dylan C. Yost [2]
[1]*Department of Physics and LAMOR, Missouri University of Science and Technology, Rolla, Missouri 65409, USA*
[2]*Department of Physics, Colorado State University, Fort Collins, Colorado 80523, USA*

(Received 23 September 2023; accepted 21 November 2023; published 26 December 2023)

The so-called proton-radius puzzle (the current discrepancy of proton radii determined from spectroscopic measurements in ordinary versus muonic hydrogen) could be addressed via an accurate measurement of the Rydberg constant because the proton radius and the Rydberg constant values are linked through high-precision optical spectroscopy. We argue that, with manageable additional experimental effort, it might be possible to improve circular Rydberg state spectroscopy, potentially leading to an important contribution to the clarification of the puzzle. Our proposal involves circular and near-circular Rydberg states of hydrogen with a principal quantum number around $n = 18$, whose classical velocity on a Bohr orbit is slower than that of the fastest macroscopic man-made object, the Parker Solar Probe. We obtain improved estimates for the quality factor of pertinent transitions and illustrate a few recent improvements in instrumentation which facilitate pertinent experiments.

DOI: 10.1103/PhysRevA.108.062822

I. INTRODUCTION

The Rydberg constant is of consummate importance for our understanding of fundamental physics. Notably, this constant is an important input datum for the calculation of transition frequencies in hydrogen and deuterium (see Table II of Ref. [1] and Refs. [2,3]). In addition to the Rydberg constant, accurate values of the proton and deuteron radii are also required in order to calculate transition frequencies in hydrogen and deuterium. Conversely, one can infer proton and deuteron radii from precise values of hydrogen and deuterium frequencies (see Refs. [1,3] and Table 45 of Ref. [2]).

With the advent of muonic hydrogen spectroscopic measurements [4,5], the Committee on Data of the International Science Council (CODATA) value of the proton radius has shifted from a 2006 value of about $R_p \approx 0.88\,\text{fm}$ to a 2018 value of about $R_p \approx 0.84\,\text{fm}$, entailing a concomitant change in the Rydberg constant [2,3]. From the 2006 to the 2018 CODATA adjustments [2,3], the Rydberg constant has shifted by much more than the uncertainty associated with the 2006 value (see Fig. 1).

One of the most attractive experimental pathways to the determination of the Rydberg constant involves transitions between two highly excited Rydberg states in atomic hydrogen, as described in Ref. [6] by a research group working at the Massachusetts Institute of Technology (MIT). Within the same group, a value for the Rydberg constant was obtained in an unpublished thesis by deVries [7] (labeled "Rydberg state" in Fig. 1),

$$cR_\infty|_{\text{deVries}} = 3\,289\,841\,960\,306(69)\,\text{kHz}. \tag{1}$$

As is evident from Fig. 1, this value is marginally consistent with both the CODATA 2006 value [2] and the 2018 CODATA value from Ref. [3]:

$$cR_\infty|_{\text{CODATA,2018}} = 3\,289\,841\,960\,250(7)\,\text{kHz}. \tag{2}$$

The 2006 CODATA value is

$$cR_\infty|_{\text{CODATA,2006}} = 3\,289\,841\,960\,360(21)\,\text{kHz}. \tag{3}$$

A comparison of the three values of the Rydberg constant is made in Fig. 1, where we use as the reference value

$$R_0 = R_\infty|_{\text{CODATA,2018}}. \tag{4}$$

The situation is interesting because, before the advent of muonic hydrogen spectroscopy, values of the Rydberg constant and of the proton radius inferred from hydrogen and deuterium spectroscopy *alone* (without any additional input from scattering experiments) were consistent with the 2006 CODATA values for both the 2006 CODATA value of the Rydberg constant and the 2006 CODATA values of the proton and deuteron radii. This is discussed in detail in the discussion surrounding Table 45 of Ref. [2], where it is pointed out that the proton radius R_p, the deuteron radius R_d, and the Rydberg constant can all be deduced using input data exclusively from hydrogen and deuterium spectroscopy.

Traditionally, the Rydberg constant has been determined on the basis of Rydberg state spectroscopy of atomic hydrogen [8–14]. An improved measurement of the Rydberg constant would thus constitute an important contribution to a resolution of the proton-radius puzzle [15]. In a remarkable investigation dating about 20 years back, circular Rydberg states around quantum numbers $n \approx 30$ were investigated with the ultimate aim of an improved measurement of the Rydberg constant [7]. Inspired by the importance of Rydberg states, it was pointed out in Refs. [16–18] that Rydberg state measurements in hydrogenlike ions of medium charge numbers could potentially offer an alternative route to the determination of the Rydberg constant.

The purpose of this paper is threefold. First, we update the calculation of the quality factors for transitions among circular Rydberg states in comparison to the estimate provided in Eq. (6) of Ref. [16]. Second, we discuss the status of quantum electrodynamic theory of Rydberg states, demonstrate that the theory is very well under control on the level of accuracy required for the determination of the Rydberg constant on the level of precision required for a resolution of the proton-radius

puzzle, and discuss the relative suppression of a number of notoriously problematic quantum electrodynamic corrections for circular and near-circular Rydberg states. Calculated values for relativistic Bethe logarithms for circular and near-circular Rydberg states with principal quantum numbers $16 \leqslant n \leqslant 20$ are also provided. Third, we provide an overview of recent advances in laser technology and other experimental techniques which facilitate an improvement of measurements of the Rydberg constant on the basis of Rydberg state measurements. Système International (SI) mksA units are employed throughout this paper.

II. QUALITY FACTORS

Of crucial importance for the feasibility of high-precision spectroscopy experiments are so-called quality factors of transitions. The quality factor is the dimensionless ratio of the transition energy to the natural linewidth of the transition (measured in radians per second), where the latter is converted to an energy via multiplication by the reduced Planck constant $\hbar$. Here, we present the general formula for the one-photon decay rate of a circular Rydberg state, with principal quantum number n and maximum orbital angular momentum quantum number $\ell = n - 1$. This reference state can decay via dipole transitions to states with principal quantum number $n - 1$ and angular momentum quantum number $\ell = n - 2$. Due to the large orbital angular momentum, neither the upper state nor the lower state of such transitions is influenced by nuclear structure effects (compare with other recently proposed schemes [19] in which the lower state is the metastable $2S$ state, which has a nonvanishing probability density at the nucleus). The calculation of radiative (dipole) decay rates of hydrogenic states is described in detail in Chap. 4 of Ref. [20] (see Gordon's formula given in Eq. (63.2) of Ref. [20]) and in Chap. 3 of Ref. [21]. For the decay rate $\gamma_n = \Gamma_n/\hbar$ of the state with principal quantum number n and maximum orbital angular momentum $\ell = n - 1$, as parameterized by the imaginary part Γ_n of the self-energy [22,23], $E = \mathrm{Re}\, E - \mathrm{i}\Gamma_n/2$, we find the result

$$\Gamma_n^{\ell=n-1} = \frac{4^{2n}(n-1)^{2n-1}\, n^{2n-4}}{(2n-1)^{4n-1}(2n-3)}\, \frac{\alpha (Z\alpha)^4 m\, c^2}{3n^5} \left(\frac{\mu}{m}\right)^3, \quad (5)$$

which can be expanded for large n as follows:

$$\Gamma_n^{\ell=n-1} = \alpha \frac{(Z\alpha)^4 mc^2}{3n^5} \left(\frac{\mu}{m}\right)^3 \left[1 + \frac{3}{2n} + \frac{17}{8n^2} + O\left(\frac{1}{n^3}\right)\right], \quad (6)$$

where m is the electron mass, μ is the reduced mass of the two-body system, α is the fine-structure constant, Z is the nuclear charge number, and the expansion for large n illustrates that the lifetimes of circular Rydberg states scale as n^5. While we have $Z = 1$ for hydrogen, we keep Z in all formulas to cover hydrogenlike ions. Also, the presence of Z in the formulas helps to distinguish the binding effects (due to the Coulomb field, with expansion parameter $Z\alpha$) from the radiative loop corrections (expansion parameter α). The energy difference for transitions among circular Rydberg states is

$$E_n - E_{n-1} = \frac{(Z\alpha)^2 \mu c^2}{2} \left(\frac{1}{(n-1)^2} - \frac{1}{n^2}\right), \quad (7)$$

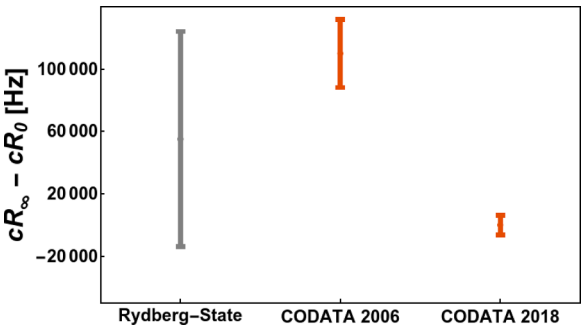

FIG. 1. We examine the values for the Rydberg constant, converted to frequency units, from CODATA adjustments and from the (unpublished, gray) result communicated in Ref. [7]. The CODATA (2006) value was reported in Ref. [2], and the CODATA (2018) value is from Ref. [3]. The reference value R_0 is from the 2018 adjustment.

which scales as $1/n^3$ for large n. Due to the $1/n^5$ asymptotics of the decay rate and the $1/n^3$ asymptotics of the transition energy, the quality factor increases for large n with the square of the principal quantum number n,

$$Q = \frac{E_n - E_{n-1}}{\Gamma_n^{\ell=n-1} + \Gamma_{n-1}^{\ell=n-2}} = \frac{3n^2}{2\alpha\,(Z\alpha)^2} \left(\frac{m}{\mu}\right)^2 \left[1 - \frac{5}{2n} - \frac{17}{8n^2} + O\left(\frac{1}{n^3}\right)\right]. \quad (8)$$

This formula constitutes an update of the estimate given in Eq. (6) of Ref. [16] (the quality factor obtained here is larger by a factor of 2 compared to Ref. [16]). The estimate in Eq. (8) illustrates the enormous advantages of Rydberg states for the measurement of the Rydberg constant. The dramatic increase of the quality factor with the square of the principal quantum number makes Rydberg state transitions very attractive. Also, we observe that the quality factor is inversely proportional to the second power of the nuclear charge number Z. This means that $Z = 1$ (atomic hydrogen) offers the best quality factor for given principal quantum number n.

Let us also evaluate the quality factor for the transition among near-circular Rydberg states, where the upper level has orbital angular momentum $\ell = n - 2$ and the lower level has orbital angular $\ell = n - 3$ (see also Fig. 2). The calculation of the quality factor proceeds in a similar way, but one needs to consider two available dipole decay channels, namely, from the reference state with principal quantum number n and orbital angular momentum quantum number $\ell = n - 2$ to lower states with $n' = n - 1$ and $\ell = n - 3$ and $n' = n - 2$ and $\ell = n - 3$. The decay width evaluates to

$$\Gamma_n^{\ell=n-2} = \alpha \frac{(Z\alpha)^4 mc^2}{3n^5} \left(\frac{\mu}{m}\right)^3 \left[1 - \frac{1}{2n} - \frac{1}{8n^2} + O\left(\frac{1}{n^3}\right)\right] + \alpha \frac{4(Z\alpha)^4 mc^2}{3n^6} \left(\frac{\mu}{m}\right)^3 \left[1 + \frac{5}{2n} + \frac{25}{4n^2} + O\left(\frac{1}{n^3}\right)\right], \quad (9)$$

where the two terms on the right-hand side correspond to the lower states with $n' = n - 1$ and $n' = n - 2$, respectively. The

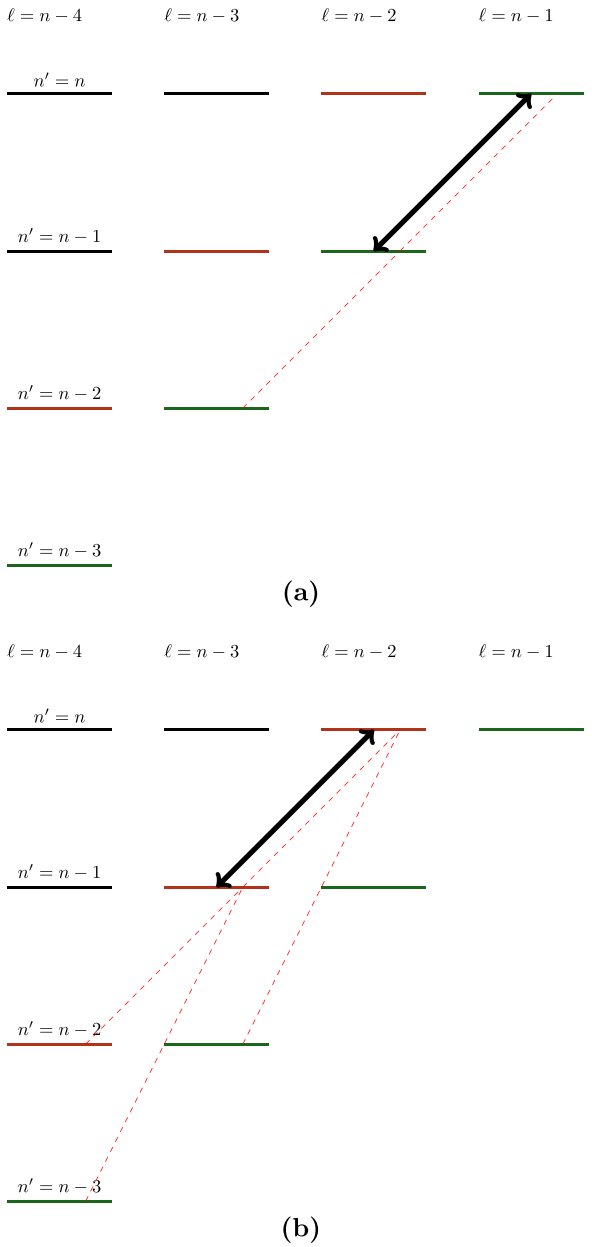

FIG. 2. The level diagram for Rydberg states illustrates the dipole-allowed transitions among (a) circular and (b) near-circular states. Circular Rydberg levels with $\ell = n-1$ are marked in green, while near-circular Rydberg levels with $\ell = n-2$ are marked in red. Transitions driven for high-precision spectroscopy are indicated with two-headed arrows. Transitions relevant for the calculation of decay rates (quality factors) are indicated by dashed lines.

quality factor evaluates to

$$Q' = \frac{E_n - E_{n-1}}{\Gamma_n^{\ell=n-2} + \Gamma_{n-1}^{\ell=n-3}} = \frac{3n^2}{2\alpha\,(Z\alpha)^2}\left(\frac{m}{\mu}\right)^2\left[1 - \frac{9}{2n} + \frac{9}{8n^2} + O\left(\frac{1}{n^3}\right)\right], \quad (10)$$

which is commensurate with Q given in Eq. (8) and illustrates that no significant accuracy loss occurs if one measures near-circular as opposed to circular Rydberg states.

A quick look at Eqs. (1), (2), and (3) and Fig. 1 illustrates that one needs to resolve the Rydberg constant to roughly one part in 10^{11} or better in order to meaningfully distinguish between the 2006 and 2018 CODATA values of the Rydberg constant. One can define a splitting factor $\mathcal{S}$, which measures the fraction to which one needs to split the resonance line in order to achieve a resolution of one part in 10^{11}. The splitting factor $\mathcal{S}$ is given by the formula

$$\mathcal{S} = 10^{11}/Q. \quad (11)$$

Again, we emphasize that it is experimentally challenging to determine the line center of a resonance line to better than ∼0.1% of its width. Therefore, an attractive option to meaningfully contribute to the proton-radius puzzle is through transitions with high quality factors, which lead to low values of the required splitting factor $\mathcal{S}$. For $Z = 1$, one obtains for $\mathcal{S}$ the perfectly reasonable figure $\mathcal{S} = 93$ for $n = 18$; expressed differently, one only needs to split the resonance lines near $n = 18$ to one part in 93 in order to achieve a resolution which meaningfully contributes to a resolution of the proton-radius puzzle.

Cross-damping terms (nonresonant corrections) can be generated by virtual levels displaced by a fine-structure interval [24]. A rough estimate of the corresponding energy (frequency) shift $\delta E_{\rm CD}$ (we set $\hbar = 1$) is given by the expression [24]

$$\delta E_{\rm CD} \sim \frac{\Gamma_n^2}{\delta E}. \quad (12)$$

Here, δE is the displacement of the virtual state responsible for the cross-damping energy shift. As pointed out in Ref. [24], the nearest virtual states which can contribute to differential cross sections are states displaced from the upper state of the Rydberg transition by a fine-structure interval. The maximum angular momentum is $\ell_{\rm max} = n-1$. The total angular momenta for the circular Rydberg states are $\ell_{\rm max} \pm 1/2$. The two possible values for the total angular momentum quantum numbers of the upper level are thus $j_+ = n - 1/2$ and $j_- = n - 3/2$, with one of these being the reference level and the other being the virtual level which contributes to the cross damping. So we have potential nonresonant contributions from virtual levels with an energy displacement

$$\delta E = E_{n,j_+} - E_{n,j_-} = \frac{(Z\alpha)^4 m}{2n^4(n-1)} \approx \frac{(Z\alpha)^4 m}{2n^5}. \quad (13)$$

The ratio of the cross-damping energy shifts relative to transition frequency is thus estimated by the expression

$$\chi \equiv \frac{\delta E_{\rm CD}}{E_n - E_{n-1}} \sim \frac{2}{9}\frac{\alpha^2 (Z\alpha)^2}{n^2}. \quad (14)$$

For $Z = 1$ and $n = 18$, this evaluates to 1.9×10^{-12}, which is less than the accuracy required to distinguish between the 2006 and 2018 CODATA values of the Rydberg constant. This estimate suggests that cross-damping effects are suppressed for Rydberg states and do not represent an obstacle for the determination of the Rydberg constant from highly excited, circular Rydberg states.

The above estimates given in Eqs. (12)–(14) are valid for the differential cross section [24]. For the total cross section, these estimates improve even further, consistent with pertinent considerations reported in Refs. [24–26].

III. QUANTUM ELECTRODYNAMIC EFFECTS

One might ask whether the theory of Rydberg state transitions is well enough under control to facilitate the interpretation of a measurement of transitions among Rydberg states. As outlined in Ref. [2], the theoretical contributions to the Lamb shift of Rydberg states on the level necessary for a determination of the Rydberg constant can be summarized into just four terms: (i) the Dirac energy (in the nonrecoil limit), which is summarized in Eq. (1) of Ref. [16], (ii) the recoil corrections from the Breit Hamiltonian, which are summarized in Eq. (2) of Ref. [16], (iii) the relativistic-recoil corrections summarized in Eq. (3) of Ref. [16], and (iv) the self-energy effect summarized in Eq. (4) of Ref. [16]. Calculated values of nonrelativistic Bethe logarithms, which enter the expression for the relativistic recoil correction, were tabulated for all states with principal quantum numbers $n \leqslant 200$ in Ref. [27]. This favorable situation illustrates the tremendous simplifications possible for Rydberg states. Notably, vacuum-polarization, nuclear-size, and nuclear-structure corrections can be completely ignored for circular Rydberg states whose probability density at the nucleus vanishes. For vacuum polarization, the energy shift due to the Uehling potential (Eq. (10.245) of Ref. [21]) is of order $\alpha(Z\alpha)^{2(n+1)}\mu c^2$ for circular Rydberg states with $\ell = n-1$ and of order $\alpha(Z\alpha)^{2n}\mu c^2$ for near-circular Rydberg states with $\ell = n-2$. Here, we are concerned with $n \geqslant 13$; effects that scale with $\alpha(Z\alpha)^{26}\mu c^2$ (or higher powers of $Z\alpha$) are numerically completely negligible. The Wichmann-Kroll potential takes into account Feynman diagrams with three and more Coulomb vertices in the fermion loop [28,29], in contrast to the Uehling potential with only one Coulomb vertex [21]. An asymptotic expression of the Wichmann-Kroll (WK) potential, valid for $r \sim a_0$ and thus applicable to circular Rydberg states (a_0 is the Bohr radius), was recently evaluated in Eq. (18.103) of Ref. [21] based on effective-field-theory methods. Its expression is given as $V_{\rm WK}(r) \approx \frac{2}{225}\,\frac{\alpha}{\pi}\,(Z\alpha)^8\mu c^2 a_0^5/r^5$. It gives rise to energy shifts that scale as $\alpha(Z\alpha)^8\mu c^2$ and are thus parametrically suppressed by four powers of the fine-structure constant in comparison to the leading self-energy effects and by two powers of the fine-structure constant in comparison to the relativistic corrections to the self-energy effects, which will be discussed below. Thus, we can neglect vacuum-polarization effects here altogether.

The most interesting radiative effect concerns the bound-state self-energy $E_{\rm SE}$, which is described by the formula (see Ref. [29] and Chap. 15 of Ref. [21])

$$E_{\rm SE} = \frac{\alpha}{\pi}\,\frac{(Z\alpha)^4\,m}{n^3}\left(A_{40} + (Z\alpha)^2 \times \left\{A_{61}\,\ln\left[\frac{m}{\mu}(Z\alpha)^{-2}\right] + A_{60}\right\}\right). \tag{15}$$

The first subscript of the A coefficients counts the number of $Z\alpha$, while the second counts the number of logarithms $\ln[\frac{m}{\mu}(Z\alpha)^{-2}]$.

The general result for the A_{40} coefficient for circular Rydberg states with orbital angular momentum $\ell \neq 0$ and principal quantum number $n \geqslant 2$ is well known,

$$A_{40} = -\left(\frac{\mu}{m}\right)^2 \frac{1}{2\kappa(2\ell+1)} - \frac{4}{3}\left(\frac{\mu}{m}\right)^3 \ln k_0(n,\ell), \tag{16}$$

where $\kappa = (-1)^{j+\ell+1/2}$ is the Dirac angular quantum number and $\ln k_0(n,\ell)$ is the Bethe logarithm. (For values of $\ln k_0(n,\ell)$, one should consult Ref. [27].) The functional dependence on the reduced mass is a consequence of the proton's convection current; an explanation is given in Chap. 12 of Ref. [21]. Here, we will place special emphasis on circular and near-circular Rydberg states with $\ell = n-1$ and $\ell = n-2$, with $n \geqslant 13$, and refer to them as the following series of states:

(i) Series $\mathcal{A}$ has $\ell = n-1$, $j{=}\ell+1/2$, $\kappa = -(j+1/2)$.
(ii) Series $\mathcal{B}$ has $\ell = n-1$, $j = \ell-1/2$, $\kappa = (j+1/2)$.
(iii) Series $\mathcal{C}$ has $\ell = n-2$, $j = \ell+1/2$, $\kappa = -(j+1/2)$.
(iv) Series $\mathcal{D}$ has $\ell = n-2$, $j = \ell-1/2$, $\kappa = (j+1/2)$.

Series $\mathcal{A}$ has the highest ℓ and j for given n. The A_{40} coefficients evaluate to the following expressions for the four series of states:

$$\frac{A_{40}(\mathcal{A},n)}{(\mu/m)^2} = \frac{1}{2n(2n-1)} - \frac{4}{3}\,\frac{\mu}{m}\,\ln k_0(n,n-1), \tag{17}$$

$$\frac{A_{40}(\mathcal{B},n)}{(\mu/m)^2} = -\frac{1}{2(n-1)(2n-1)} - \frac{4}{3}\,\frac{\mu}{m}\,\ln k_0(n,n-1), \tag{18}$$

$$\frac{A_{40}(\mathcal{C},n)}{(\mu/m)^2} = \frac{1}{2(n-1)(2n-3)} - \frac{4}{3}\,\frac{\mu}{m}\,\ln k_0(n,n-2), \tag{19}$$

$$\frac{A_{40}(\mathcal{D},n)}{(\mu/m)^2} = -\frac{1}{2(n-2)(2n-3)} - \frac{4}{3}\,\frac{\mu}{m}\,\ln k_0(n,n-2). \tag{20}$$

As a function of the principal quantum number, the Bethe logarithms $\ln k_0(n,n-1)$ and $\ln k_0(n,n-2)$ decrease with n for large n as n^{-3}. In the nonrecoil limit $\mu \to m$ and the limit of large n, one has

$$A_{40}(\mathcal{A},n) \approx -A_{40}(\mathcal{B},n) \approx A_{40}(\mathcal{C},n) \approx -A_{40}(\mathcal{D},n) \approx \frac{1}{4n^2}, \qquad n \to \infty. \tag{21}$$

The leading quantum electrodynamic corrections for circular and near-circular Rydberg states are parameterized by the A_{40} coefficient. The quantum electrodynamic effects are seen to be suppressed, for large n, by a factor of n^{-2} which appears in addition to the overall scaling factor n^{-3} in Eq. (15).

Higher-loop contributions to the anomalous magnetic moment can be taken into account by the replacement

$$-\left(\frac{\mu}{m}\right)^2 \frac{1}{2\kappa(2\ell+1)} \to -\left(\frac{\mu}{m}\right)^2 \frac{1}{2\kappa(2\ell+1)}\,\frac{a_e}{\alpha/(2\pi)}, \tag{22}$$

where a_e contains the higher-loop contributions to the electron anomalous magnetic moment, which determines the g factor of the electron according to $g = 2(1+a_e)$. The term $\alpha/(2\pi)$ is the one-loop Schwinger value [30]. The quantity a_e can be taken either as the most recent experimental value of the electron anomalous magnetic moment [31], which results in $a_e = 1.159\,652\,180\,59(13) \times 10^{-3}$, or as a purely theoretical prediction including higher-order effects [32].

The suppression of the quantum electrodynamic effects for circular and near-circular Rydberg states has a physical reason which is connected to the slow velocity of electrons on highly excited near-circular Bohr orbits. Namely, the velocity of a classical electron orbiting the nucleus in a Bohr orbit corresponding to the principal quantum number n is

$$v_{\rm cl} = \frac{Z\alpha c}{n}. \tag{23}$$

The ratio $v_{\rm cl}/c = Z\alpha/n$ is thus additionally suppressed with respect to the usual expansion parameter $Z\alpha$ of bound-state quantum electrodynamics by an additional inverse power of n. The effective expansion parameter for Rydberg states is thus, strictly speaking, not $Z\alpha$, but, more precisely, $Z\alpha/n$. The persistence of the principal quantum number n in the denominator of the expansion parameter is evident not only in the nonrelativistic Schrödinger-Coulomb spectrum but also in the Dirac-Coulomb binding energy, that is, the solution of the relativistic Dirac equation coupled to the Coulomb field. For reference (see Eq. (8.49e) of Ref. [21]), the bound-state Dirac-Coulomb energy E fulfills $E/m = f(n, j)$, where $f(n, j) = [1 + (Z\alpha/\bar{n})^2]^{-1/2}$. Here, $\bar{n} = n - |j + 1/2| + \sqrt{(j + 1/2)^2 - (Z\alpha)^2}$ fulfills $\bar{n} = n - (Z\alpha)^2/(2|j + 1/2|) + O(Z\alpha)^4$ and thus $\bar{n} \approx n$ for large n and j. The approximate formula $f(n, j) \approx [1 + (Z\alpha/n)^2]^{-1/2}$ exhibits the effective expansion parameter $Z\alpha/n$.

The classical velocity $v_{\rm cl}$ evaluates, for $Z = 1$ and $n = 18$ (this choice of n is explained in Sec. IV), to a velocity of 1.21×10^5 m/s. This is slower than the velocity of the fastest macroscopic man-made object, namely, the Parker Solar Probe, which recently reached a velocity of 1.48×10^5 m/s on its orbit around the Sun [33,34]. Effects originating from relativity and quantum electrodynamics are thus highly suppressed for circular Rydberg states. Furthermore, the slow speed of the bound electrons in comparison to macroscopic, gravitationally bound systems is interesting in view of the weakness of gravitational interactions in general; the comparison illustratively demonstrates the weak binding of Rydberg electrons, which makes them suitable for high-precision determinations of the Rydberg constant.

The general result for the A_{61} coefficient, valid for Rydberg states with $n \geqslant 13$ and $\ell = n - 1$ and $\ell = n - 2$, was given in Eq. (6) of Ref. [35] and Eq. (4) of Ref. [16] and reads

$$A_{61} = \left(\frac{\mu}{m}\right)^3 \frac{3n^2 - \ell(\ell+1)}{3n^2(\ell+3/2)(\ell+1)(\ell+1/2)\ell(\ell-1/2)}, \tag{24}$$

a result which is independent of the spin orientation. This expression evaluates to

$$\frac{A_{61}(\mathcal{A}, n)}{(\mu/m)^3} = \frac{A_{61}(\mathcal{B}, n)}{(\mu/m)^3} = \frac{8}{3n^2(n-1)(2n-1)(2n-3)}, \tag{25}$$

$$\frac{A_{61}(\mathcal{C}, n)}{(\mu/m)^3} = \frac{A_{61}(\mathcal{D}, n)}{(\mu/m)^3} = \frac{32(n+2)}{3n^2\prod_{i=2}^{5}(2n-i)}. \tag{26}$$

In the large-n limit, one has

$$A_{61}(\mathcal{A}, n) \approx A_{61}(\mathcal{B}, n) \approx A_{61}(\mathcal{C}, n) \approx A_{61}(\mathcal{D}, n) \approx \frac{2}{3n^5}, \quad n \to \infty. \tag{27}$$

TABLE I. Calculated values for the A_{60} coefficients for highly excited Rydberg states for the $\mathcal{A}$, $\mathcal{B}$, $\mathcal{C}$, and $\mathcal{D}$ series of states for principal quantum numbers $16 \leqslant n \leqslant 20$.

			$\mathcal{A}$ series		$\mathcal{B}$ series
n	ℓ	j	$A_{60}(n\ell_j)$	j	$A_{60}(n\ell_j)$
16	15	$\frac{31}{2}$	$1.059\,675(5) \times 10^{-5}$	$\frac{29}{2}$	$0.121\,748(5) \times 10^{-5}$
17	16	$\frac{33}{2}$	$0.805\,212(5) \times 10^{-5}$	$\frac{31}{2}$	$0.078\,287(5) \times 10^{-5}$
18	17	$\frac{35}{2}$	$0.621\,952(5) \times 10^{-5}$	$\frac{33}{2}$	$0.049\,885(5) \times 10^{-5}$
19	18	$\frac{37}{2}$	$0.487\,434(5) \times 10^{-5}$	$\frac{35}{2}$	$0.031\,113(5) \times 10^{-5}$
20	19	$\frac{39}{2}$	$0.387\,025(5) \times 10^{-5}$	$\frac{37}{2}$	$0.018\,584(5) \times 10^{-5}$
			$\mathcal{C}$ series		$\mathcal{D}$ series
n	ℓ	j	$A_{60}(n\ell_j)$	j	$A_{60}(n\ell_j)$
16	14	$\frac{29}{2}$	$1.540\,182(5) \times 10^{-5}$	$\frac{27}{2}$	$0.155\,784(5) \times 10^{-5}$
17	15	$\frac{31}{2}$	$1.145\,325(5) \times 10^{-5}$	$\frac{29}{2}$	$0.096\,026(5) \times 10^{-5}$
18	16	$\frac{33}{2}$	$0.867\,820(5) \times 10^{-5}$	$\frac{31}{2}$	$0.058\,328(5) \times 10^{-5}$
19	17	$\frac{35}{2}$	$0.668\,553(5) \times 10^{-5}$	$\frac{33}{2}$	$0.034\,217(5) \times 10^{-5}$
20	18	$\frac{37}{2}$	$0.522\,676(5) \times 10^{-5}$	$\frac{35}{2}$	$0.018\,690(5) \times 10^{-5}$

The suppression with n^{-5}, in addition to the overall scaling factor n^{-3} from Eq. (15), again illustrates the smallness of relativistic and quantum electrodynamic effects for circular Rydberg states.

The next higher coefficient is A_{60}, which is called the relativistic Bethe logarithm [36,37]. Its absolute magnitude is highly suppressed for circular Rydberg states. Specifically, according to Refs. [16–18] and Table 7.2 of Ref. [38], one has

$$\max\{|A_{60}(\mathcal{A}, n)|, |A_{60}(\mathcal{B}, n)|, \times |A_{60}(\mathcal{C}, n)|, |A_{60}(\mathcal{D}, n)|\} < 10^{-4}, \quad n > 13. \tag{28}$$

Furthermore, according to the calculations reported in Refs. [18,39], the approximation $G_{\rm SE} \approx A_{60}$ for the nonperturbative self-energy remainder function remains valid to excellent approximation for circular Rydberg states for low and medium nuclear charge numbers (see Table 1 of Ref. [39] and Tables 1 and 2 of Ref. [18]). Relation (28) implies that the correction to the transition frequency among circular Rydberg states induced by the relativistic Bethe logarithm A_{60} for $Z = 1$ is smaller than one part in 10^{-15} for $n \geqslant 13$. Nevertheless, it is useful to calculate numerical values of relativistic Bethe logarithms for the states under investigation here (see Table I). We follow the calculational procedure outlined in Ref. [35]. For calculated values of A_{60} for circular and near-circular Rydberg states with $13 \leqslant n \leqslant 16$, we refer to Table 1 of Ref. [16] and Table 1 Ref. [18].

IV. EXPERIMENTAL CONSIDERATIONS

Let us also include a few considerations relevant to the experimental realization of a high-precision measurement of the Rydberg constant based on circular Rydberg states. One might assume that ultimate experimental success could be

bolstered by choosing transitions with as high a quality factor Q as possible. As discussed around Eq. (8), since $Q \propto n^2$, high n is desirable.

However, it is also important to consider the sensitivity of a given measurement to systematic effects. Many systematic effects increase with powers of n. For instance, shifts and distortions of resonances due to the Stark effect scale as n^5 [7,40,41], which produces challenges to measuring transitions between circular Rydberg states with very high n. However, the previous measurement between circular Rydberg states of hydrogen [7] between $n = 27$ and $n = 28$ and between $n = 29$ and $n = 30$ had negligible contributions from uncertainties in the Stark shifts [7]. The experimental accuracy was instead limited by dipole-dipole interactions. Since the dipole moment for an atom in a superposition of adjacent circular Rydberg states scales as n^2 and the systematic effect is related to the interaction energy of two dipoles, this effect scales as n^4.

Therefore, in order to mitigate the dipole-dipole interactions, it may be interesting to consider transitions between circular Rydberg states with somewhat lower n. For instance, with all other experimental parameters being similar, a transition between $n = 18$ and $n = 19$ would reduce the effects of the dipole-dipole interactions by a factor of $\sim$6 compared to the previous measurement [7]. Another experimental benefit to reducing n below that demonstrated in [7] is that blackbody-radiation-induced transitions would be mitigated because the thermal radiation spectral density for temperatures $\leqslant 300$ K is reduced for the more energetic transitions occurring between lower-lying states. This may allow the experiment to be performed at liquid-nitrogen as opposed to liquid-helium temperatures.

The MIT measurement [7] used pulsed lasers at a repetition rate of 61 Hz to produce circular Rydberg states. Therefore, another option to mitigate dipole-dipole interactions could be to produce a near-continuous source of circular Rydberg states using continuous-wave (cw) lasers. Since the dipole-dipole interaction is related to the peak density of circular Rydberg states, a near-continuous source of circular Rydberg states could allow for a large reduction in the peak density while maintaining sufficient statistics. This could be accomplished by first using the $1S$–$2S$ two-photon transition to populate the $2S$ metastable state as in Refs. [42,43], followed by excitation to Rydberg levels using a 365-nm cw laser. Then circularization would be performed using the methods outlined in Ref. [6]. The use of a cw rather than a pulsed laser for the excitation into the Rydberg states [44] constitutes the main technological advancement over the methods used in Ref. [7]; its use could lead to a drastic increase in the number of available Rydberg atoms and thus drastically improved statistics with simultaneously reduced systematic effects due to lower peak Rydberg atom density.

To perform spectroscopy of the $n = 18$ to $n = 19$ circular Rydberg states, a millimeter-wave Ramsey apparatus akin to the one employed in Ref. [7] could be used. To excite the transition, a radiation source at 1.04 THz is needed. While the millimeter-wave source in [7] operated at 256 or 316 GHz, a similar source operating at frequencies above 1 THz is possible using a planar GaAs Schottky diode frequency multiplier [45]. The output power of such terahertz sources is relatively low. However, due to the large transition matrix element between circular Rydberg states, the transition can be saturated with <1 nW and a 3-mm beam waist. Therefore, commercially available terahertz sources would likely be sufficient [46].

V. CONCLUSIONS

The main conclusions of this paper are as follows. In Sec. II, we showed that the quality factors of transitions among circular Rydberg are sufficient to comfortably allow for a distinction between the 2006 and 2018 CODATA values of the Rydberg constant (see Eqs. (2) and (3) and Refs. [2,3]). Furthermore, according to the considerations reported in Sec. II, cross-damping terms do not present an obstacle to such a measurement. In Sec. III, we showed that the theory of bound states is sufficiently under control to allow for a determination of the Rydberg constant from transitions among circular Rydberg states in atomic hydrogen. Experimental considerations (Sec. IV) corroborate the advances in technology which make such a measurement more feasible than reported in Ref. [7], in part by reducing several systematic effects through a less dense atomic beam which can be realized in a continuous-wave excitation scheme into the circular states.

A few concluding remarks on the proton-radius puzzle are in order. We recall that the proton-radius puzzle refers to the difference between the "smaller" proton radius of $R_p \approx 0.84\,\text{fm}$ obtained in Ref. [4] and the larger value of $R_p \approx 0.88\,\text{fm}$ from the 2006 CODATA adjustment (see Refs. [1,2,12,13] and references therein). Various recent scattering experiments [47,48] and spectroscopic experiments [42,43,49–51] came to conflicting conclusions on the proton radius. A recent measurement described in Refs. [43] led to a value of $R_p \approx 0.86\,\text{fm}$. It was very recently pointed out in Ref. [15] that two older scattering experiments, carried out in 1969 at Brookhaven (see Refs. [52,53]), are consistent with an 8% discrepancy in the cross sections between muon-proton and electron-proton scattering, which translates into 4% for the form-factor slope, which in turn amounts to 2% for the radius. This is precisely the difference between the smaller proton radius of $R_p \approx 0.84\,\text{fm}$ and the recently obtained [43] value of $R_p \approx 0.86\,\text{fm}$. The MUon proton Scattering Experiment (MUSE) experiment [54–56] at the Paul Scherrer Institute (PSI) aims to remeasure the muon-proton cross sections in the near future.

In conclusion, we have shown that the idea formulated in Refs. [6,7,16–18,40,41] could lead to a feasible pathway toward a determination of the Rydberg constant. This could be interesting because most recent spectroscopic experiments [42,43,49–51] focus on transitions in atomic hydrogen which depend on both constants in question, namely, the proton radius and the Rydberg constant. Focusing on Rydberg states, as proposed here, means that one isolates one of these constants, thereby potentially obtaining a clear and distinct picture of the proton-radius puzzle. The current situation provides motivation not only to carry out the MUSE experiment at PSI [54–56] but also to redouble efforts to measure the Rydberg constant.

ACKNOWLEDGMENTS

The authors acknowledge extensive insightful conversations with B. J. Wundt and helpful conversations with S. M. Brewer. Support from the National Science Foundation (Grant No. PHY–2110294) is gratefully acknowledged. Furthermore, U.D.J. and D.C.Y. gratefully acknowledge support from the Templeton Foundation (Fundamental Physics Black Grant, Subawards 60049570 MST and 60049570 CSU of Grant ID No. 61039).

[1] U. D. Jentschura, S. Kotochigova, E.-O. Le Bigot, P. J. Mohr, and B. N. Taylor, Precise calculation of transition frequencies of hydrogen and deuterium based on a least-squares analysis, Phys. Rev. Lett. **95**, 163003 (2005).

[2] P. J. Mohr, B. N. Taylor, and D. B. Newell, CODATA recommended values of the fundamental physical constants: 2006, Rev. Mod. Phys. **80**, 633 (2008).

[3] E. Tiesinga, P. J. Mohr, D. B. Newell, and B. N. Taylor, CODATA recommended values of the fundamental physical constants: 2018, Rev. Mod. Phys. **93**, 025010 (2021).

[4] R. Pohl *et al.*, The size of the proton, Nature (London) **466**, 213 (2010).

[5] R. Pohl *et al.*, Laser spectroscopy of muonic deuterium, Science **353**, 669 (2016).

[6] R. Lutwak, J. Holley, P. P. Chang, S. Paine, D. Kleppner, and T. Ducas, Circular states of atomic hydrogen, Phys. Rev. A **56**, 1443 (1997).

[7] J. C. deVries, A precision millimeter–wave measurement of the Rydberg frequency, Ph.D. thesis, Massachusetts Institute of Technology, 2002.

[8] B. P. Kibble, W. R. C. Rowley, R. E. Shawyer, and G. W. Series, An experimental determination of the Rydberg constant, J. Phys. B **6**, 1079 (1973).

[9] T. F. Gallagher, *Rydberg Atoms* (Cambridge University Press, Cambridge, UK, 1994).

[10] F. Biraben, J.-C. Garreau, L. Julien, and M. Allegrini, New measurement of the Rydberg constant by two-photon spectroscopy of hydrogen Rydberg states, Phys. Rev. Lett. **62**, 621 (1989).

[11] F. Nez, M. D. Plimmer, S. Bourzeix, L. Julien, F. Biraben, R. Felder, O. Acef, J. J. Zondy, P. Laurent, A. Clairon, M. Abed, Y. Millerioux, and P. Juncar, Precise frequency measurement of the $2S$-$8S/8D$ transitions in atomic hydrogen: New determination of the Rydberg constant, Phys. Rev. Lett. **69**, 2326 (1992).

[12] B. de Beauvoir, F. Nez, L. Julien, B. Cagnac, F. Biraben, D. Touahri, L. Hilico, O. Acef, A. Clairon, and J. J. Zondy, Absolute frequency measurement of the $2S$–$8S/D$ transitions in hydrogen and deuterium: New determination of the Rydberg constant, Phys. Rev. Lett. **78**, 440 (1997).

[13] C. Schwob, L. Jozefowski, B. de Beauvoir, L. Hilico, F. Nez, L. Julien, F. Biraben, O. Acef, J. J. Zondy, and A. Clairon, Optical frequency measurement of the $2S$-$12D$ transitions in hydrogen and deuterium: Rydberg constant and lamb shift determinations, Phys. Rev. Lett. **82**, 4960 (1999); **86**, 4193(E) (2001).

[14] B. de Beauvoir, C. Schwob, O. Acef, L. Jozefowski, L. Hilico, F. Nez, L. Julien, A. Clairon, and F. Biraben, Metrology of the hydrogen and deuterium atoms: Determination of the Rydberg constant and Lamb shifts, Eur. Phys. J. D **12**, 61 (2000).

[15] U. D. Jentschura, Proton Rradius: A puzzle or a solution!? J. Phys.: Conf. Ser. **2391**, 012017 (2022).

[16] U. D. Jentschura, P. J. Mohr, J. N. Tan, and B. J. Wundt, Fundamental constants and tests of theory in Rydberg states of hydrogen-like ions, Phys. Rev. Lett. **100**, 160404 (2008).

[17] U. D. Jentschura, P. J. Mohr, J. N. Tan, and B. J. Wundt, Fundamental constants and tests of theory in Rydberg states of hydrogenlike ions, Can. J. Phys. **87**, 757 (2009).

[18] U. D. Jentschura, P. J. Mohr, and J. N. Tan, Fundamental constants and tests of theory in Rydberg states of one-electron ions, J. Phys. B **43**, 074002 (2010).

[19] S. Scheidegger, J. A. Agner, H. Schmutz, and F. Merkt, Metrology of Rydberg states of the hydrogen atom, arXiv:2309.12721.

[20] H. A. Bethe and E. E. Salpeter, *Quantum Mechanics of One- and Two-Electron Atoms* (Springer, Berlin, 1957).

[21] U. D. Jentschura and G. S. Adkins, *Quantum Electrodynamics: Atoms, Lasers and Gravity* (World Scientific, Singapore, 2022).

[22] U. D. Jentschura, Non-uniform convergence of two-photon decay rates for excited atomic states, J. Phys. A **40**, F223 (2007).

[23] U. D. Jentschura, Two-photon decays reexamined: Cascade contributions and gauge invariance, J. Phys. A **41**, 155307 (2008).

[24] U. D. Jentschura and P. J. Mohr, Nonresonant effects in one–and two–photon transitions, Can. J. Phys. **80**, 633 (2002).

[25] F. Low, Natural line shape, Phys. Rev. **88**, 53 (1952).

[26] T. Udem, L. Maisenbacher, A. Matveev, V. Andreev, A. Grinin, A. Beyer, N. Kolachevsky, R. Pohl, D. C. Yost, and T. W. Hänsch, Quantum interference line shifts of broad dipole-allowed transitions, Ann. Phys. (Berlin, Ger.) **531**, 1900044 (2019).

[27] U. D. Jentschura and P. J. Mohr, Calculation of hydrogenic Bethe logarithms for Rydberg states, Phys. Rev. A **72**, 012110 (2005).

[28] E. H. Wichmann and N. M. Kroll, Vacuum polarization in a strong Coulomb field, Phys. Rev. **96**, 232 (1954).

[29] M. I. Eides, H. Grotch, and V. A. Shelyuto, Theory of light hydrogenlike atoms, Phys. Rep. **342**, 63 (2001).

[30] J. Schwinger, On quantum-electrodynamics and the magnetic moment of the electron, Phys. Rev. **73**, 416 (1948).

[31] X. Fan, T. G. Myers, B. A. D. Sukra, and G. Gabrielse, Measurement of the electron magnetic moment, Phys. Rev. Lett. **130**, 071801 (2023).

[32] S. Laporta, High-precision calculation of the 4-loop QED contribution to the slope of the Dirac form factor, Phys. Lett. B **800**, 135137 (2020).

[33] CNET: NASA solar probe becomes fastest object ever built as it 'touches the sun,' https://www.cnet.com/science/space/nasa-solar-probe-becomes-fastest-object-ever-built-as-it-touches-the-sun/.

[34] N. E. Raouafi *et al.*, Parker Solar Probe: Four years of discoveries at solar cycle minimum, Space Sci. Rev. **219**, 8 (2023).

[35] B. J. Wundt and U. D. Jentschura, Reparameterization invariance of NRQED self-energy corrections and improved theory for excited D states in hydrogenlike systems, Phys. Lett. B **659**, 571 (2008).

[36] U. D. Jentschura, E.-O. Le Bigot, P. J. Mohr, P. Indelicato, and G. Soff, Asymptotic properties of self-energy coefficients, Phys. Rev. Lett. **90**, 163001 (2003).

[37] E.-O. Le Bigot, U. D. Jentschura, P. J. Mohr, P. Indelicato, and G. Soff, Perturbation approach to the self-energy of non-S hydrogenic states, Phys. Rev. A **68**, 042101 (2003).

[38] B. J. Wundt, Quantum electrodynamics and fundamental constants, Ph.D. thesis, Missouri University of Science and Technology, 2011.

[39] B. J. Wundt and U. D. Jentschura, Proposal for the determination of nuclear masses by high-precision spectroscopy of Rydberg states, J. Phys. B **43**, 115002 (2010).

[40] R. Lutwak, Millimeter-wave studies of hydrogen Ryberg states, Ph.D. thesis, Massachusetts Institute of Technology, 1988.

[41] J. R. Holley, Precision spectroscopy of circular Rydberg states of hydrogen, Ph.D. thesis, Massachusetts Institute of Technology, 1998.

[42] A. Beyer, L. Maisenbacher, A. Matveev, R. Pohl, K. Khabarova, A. Grinin, T. Lamour, D. C. Yosta, T. W. Hänsch, N. Kolachevsky, and Th. Udem, The Rydberg constant and proton size from atomic hydrogen, Science **358**, 79 (2017).

[43] A. D. Brandt, S. F. Cooper, C. Rasor, Z. Burkley, A. Matveev, and D. C. Yost, Measurement of the $2S_{1/2}$–$8D_{5/2}$ transition in hydrogen, Phys. Rev. Lett. **128**, 023001 (2022).

[44] Z. Burkley, A. D. Brandt, C. Rasor, S. F. Cooper, and D. C. Yost, Highly coherent, Watt-level deep-UV radiation via a frequency-quadrupled Yb-fiber laser system, Appl. Opt. **58**, 1657 (2019).

[45] I. Mehdi, J. V. Siles, C. Lee, and E. Schlecht, THz Diode technology: Status, prospects, and applications, Proc. IEEE **105**, 990 (2017).

[46] https://www.vadiodes.com/.

[47] J. C. Bernauer *et al.*, High-precision determination of the electric and magnetic form factors of the proton, Phys. Rev. Lett. **105**, 242001 (2010).

[48] W. Xiong *et al.*, A small proton charge radius from an electron-proton scattering experiment, Nature (London) **575**, 147 (2019).

[49] H. Fleurbaey, S. Galtier, S. Thomas, M. Bonnaud, L. Julien, F. Biraben, F. Nez, M. Abgrall, and J. Guéna, New measurement of the 1S–3S transition frequency of hydrogen: Contribution to the proton charge radius puzzle, Phys. Rev. Lett. **120**, 183001 (2018).

[50] N. Bezginov, T. Valdez, M. Horbatsch, A. Marsman, A. C. Vutha, and E. A. Hessels, A measurement of the atomic hydrogen Lamb shift and the proton charge radius, Science **365**, 1007 (2019).

[51] P. Yzombard, S. Thomas, L. Julien, F. Biraben, and F. Nez, 1S-3S cw spectroscopy of hydrogen/deuterium atom, Eur. Phys. J. D **77**, 23 (2023).

[52] L. Camilleri, J. H. Christenson, M. Kramer, L. M. Lederman, Y. Nagashima, and T. Yamanouchi, High–energy muon–proton scattering: One–photon exchange test, Phys. Rev. Lett. **23**, 149 (1969).

[53] L. Camilleri, J. H. Christenson, M. Kramer, L. M. Lederman, Y. Nagashima, and T. Yamanouchi, High-energy muon-proton scattering: Muon-electron universality, Phys. Rev. Lett. **23**, 153 (1969).

[54] https://www.psi.ch/en/muse/experiment.

[55] M. Kohl *et al.* (MUSE Collaboration), Muon elastic scattering with MUSE at PSI, Eur. Phys. J. Web Conf. **66**, 06010 (2014).

[56] M. Kohl (private communication).